Available online at www.sciencedirect.com
SCIENCE DIRECT®

Journal of the European Ceramic Society 23 (2003) 2747–2759
www.elsevier.com/locate/jeurceramsoc

Gibbs' adsorption at α alumina–copper interfaces

Monika Backhaus-Ricoult[a,b,*]

[a]Centre d'Etudes de Chimie Metallurgique, CNRS, 15 Rue G. Urbain, 94407 Vitry, France
[b]Department of Materials Science and Engineering, Cornell University, Ithaca, NY 14853, USA

Abstract

Gibbs adsorption isotherms of oxygen to α alumina–transition metal interfaces are derived from a point defect model that handles chemical interactions and crystallographic structure at the interface. The model considers structural vacancies and interfacial charge transfer clusters as characteristic interfacial point defects. Majority defect type and concentrations strongly depend on the oxygen activity. Adsorption isotherms are derived for typical data sets for liquid and for solid copper in contact with alumina, revealing three adsorption ranges: adsorption-free interfaces in an intermediate oxygen activity range, interfaces with oxygen excess in form of interfacial oxide charge transfer clusters at high oxygen activity and oxygen deficient interfaces with interfacial metal clusters at low oxygen activity. The model predicts differences in adsorption behavior for crystallographically different interfaces; ''polarity'' and atom density in the interfacial oxide plane play key roles. Model predictions are confronted to literature results on the wetting behavior of alumina by liquid copper and to EELS investigations on the interfacial bonding in the solid Cu–alumina system.

Keywords: Alumina; Copper; Interfaces

1. Introduction

Phenomena of adsorption to surfaces and interfaces were already treated by Gibbs in 1878,[1] lead to his well-known adsorption isotherms and, since then, have been applied to numerous systems. The Gibbs' adsorption theory is based on continuum thermodynamics and can easily be applied to liquid surfaces and interfaces, however, it needs revision when being applied to crystalline materials. Upon adsorption from liquid or gas phases to crystalline surfaces, stresses are readily relaxed by the viscous phase and adsorption often follows a simple Langmuir isotherm

$$\mathrm{SO} = \mathrm{A}\cdot p_{\mathrm{O2}}^{1/2}\mathrm{e}^{-E\mathrm{ads}/RT}/\left(1+\ p_{\mathrm{O2}}^{1/2}\mathrm{e}^{-E\mathrm{ads}/RT}\right)+\mathrm{B};\qquad \mathrm{A},\mathrm{B}=\text{constants} \tag{1}$$

for the reaction

$$\mathrm{SV}+1/2\ \mathrm{O}_2=\mathrm{SO}, \tag{2}$$

with SV the number of empty adsorption sites on the surface, SO that of oxygen-occupied sites, and SO + SV = constant.

For crystalline interfaces, stresses are generated upon adsorption and cannot easily be relaxed because of matter, charge and lattice conservation in the two crystals. Even though falsely suggested by Eq. (2), the crystal lattice is not an extensive thermodynamic variable and lattice sites cannot be treated like chemical species. Thermodynamic compounds, such as alumina, are made of chemical components *i* (aluminum and oxygen) with chemical potential μ_i. In case of coexisting alumina and metallic copper phases, according to the Gibbs' phase rule,[2] the number of independent components is 1. The coexisting crystals contain different defects and regular species, their structural units, that are characterized by their chemical nature, lattice site and charge. These structural units exist only in the crystal, but not outside, therefore they can be attributed only with a virtual chemical potential. Reactions within the crystal or between different crystalline phases can be expressed in terms of these structural units. In order to associate an energy to the reaction, it is necessary to consider combinations of structural units, which are building units of the crystal (possess the lattice occupation and the global charge of the regular crystal

* Tel.: +1-33-1-46-87-35-93; fax: +1-33-46-75-04-33.
E-mail address: monika@ccmr.cornell.edu (M. Backhaus-Ricoult).

0955-2219/03/$ - see front matter © 2003 Elsevier Ltd. All rights reserved.
doi:10.1016/S0955-2219(03)00286-3

molecule) and have measurable, tabulated chemical potentials.

While this formal concept of lattice thermodynamics has been used to handle point defect thermodynamics, matter transport and solid state reactions between different oxides,[3] it has not been applied to adsorption reactions to metal-oxide interfaces, where mass, site and charge balances and the fact that the crystals share no common sublattice make the problem challenging.

General concepts for adsorption to metal-oxide interfaces were presented,[4] ab inito calculations performed for Nb–alumina,[5] and the Gibbs' adsorption concept was applied by the present author to metal–oxide interfaces in,[6] deriving predictions for MgO–Cu interfaces,[7,8] however, in that latter model, effects of adsorption-related stresses were not considered. In the present work, adsorption stresses are evaluated for Gibbs' adsorption to alumina–copper interfaces. We define the thermodynamic basics (Section 2), give a classification of low energy interfaces between α-alumina (R3c) and cubic metal and retain three characteristic types of interfaces (Section 3) and formulate the various adsorption reactions at the interface (Section 4). Then we discuss in Section 5 different approximations for the adsorption energies and show the resulting adsorption isotherms. In a final Section 6, we compare the model predictions to literature results on wetting of alumina by liquid copper and EELS investigations on the bonding at solid copper–alumina interfaces.

2. Thermodynamic consideration of the copper–alumina interface

In the present phenomenological approach, the transition metal-alumina interface is considered as a four-slab system made of bulk metal, interfacial metal slab, interfacial oxide slab and bulk oxide, Fig. 1. Bulk phases, (met) and (ox), interfacial slabs (if-met and if-ox) and surrounding gas phase (gas) are in thermodynamic equilibrium; as a consequence, the chemical potential of the components in the different slabs and in the gas phase are the same:

$$\mu_i^{(\mathrm{met})} = \mu_i^{(\mathrm{if})} = \mu_i^{(\mathrm{ox})} = \mu_i^{(\mathrm{gas})} \tag{3}$$

For the coexistence of alumina and copper, oxygen is chosen as the independent component; chemical potentials and concentrations of copper and aluminum are linked to it through the Gibbs Duhem equation and the phase formation conditions. For oxygen, we can write:

$$\begin{aligned}\mu_{\mathrm{O}}^{(\mathrm{if\text{-}met})} &= \mu_{\mathrm{O}}^{\circ(\mathrm{if\text{-}met})} + R\mathrm{T}\ \ln\ a_{\mathrm{O}}^{(\mathrm{if\text{-}met})} \\ &= \mu_{\mathrm{O}}^{\circ(\mathrm{met})} + RT\ \ln\ a_{\mathrm{O}}^{(\mathrm{met})} = \mu_{\mathrm{O}}^{(\mathrm{if\text{-}ox})} \\ &= \mu_{\mathrm{O}}^{\circ(\mathrm{if\text{-}ox})} + \mathrm{RT}\ \ln\ a_{\mathrm{O}}^{(\mathrm{if\text{-}ox})} \\ &= \mu_{\mathrm{O}}^{\circ(\mathrm{ox})} + RT\ \ln\ a_{\mathrm{O}}^{(\mathrm{ox})} \\ &= 0.5\mu_{\mathrm{O2}}^{\circ(\mathrm{gas})} + 0.5\ RT\ \ln\ a_{\mathrm{O2}}^{(\mathrm{gas})}\end{aligned} \tag{4}$$

with $\Delta G^{\circ\mathrm{ads}} = \mu_{\mathrm{O2}}^{\circ(\mathrm{g})} - \mu_{\mathrm{O}}^{\circ(\mathrm{if})}$ being the adsorption energy for oxygen from the gas to the interfacial slabs, $\Delta G^{\circ\mathrm{sol}} = \mu_{\mathrm{O2}}^{\circ(\mathrm{g})} - \mu_{\mathrm{O}}^{\circ(\mathrm{met})}$ the solution energy for oxygen to be dissolved from the gas into the metal and $\Delta G^{\circ\mathrm{seg}} = \mu_{\mathrm{O2}}^{\circ(\mathrm{met\ or\ oxide})} - \mu_{\mathrm{O}}^{\circ(\mathrm{if})}$ the energy of segregation for oxygen from the bulk metal (oxide) to the interface. μ_i° are the standard chemical potential of the pure substances, a_i the activities, R the gas constant and T the temperature.

From (4) follows

$$\begin{aligned}a_{\mathrm{O}}^{(\mathrm{if\text{-}met})} &= a_{\mathrm{O2}}^{(\mathrm{g})1/2}\exp\left(-\Delta G^{\circ\mathrm{adsmet}}/RT\right) \\ &= a_{\mathrm{O}}^{(\mathrm{met})}\exp\left(-\Delta G^{\circ\mathrm{segmet}}/RT\right)\end{aligned} \tag{5a}$$

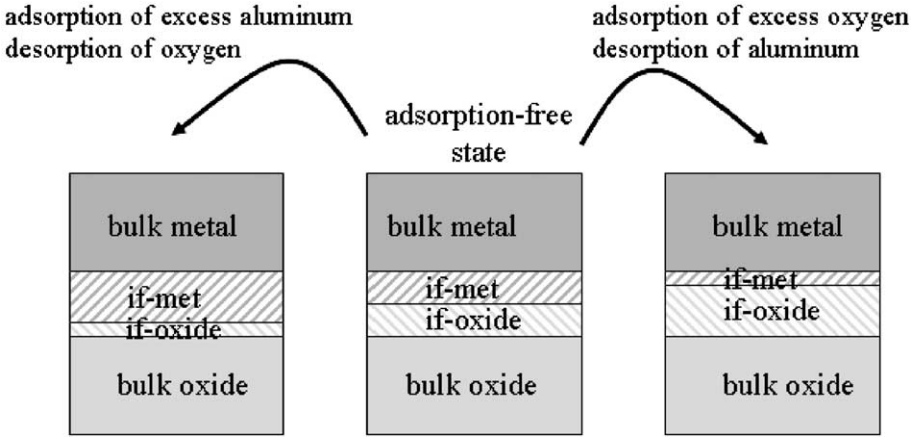

Fig. 1. Four slab metal–oxide interface, for relative oxygen deficiency (left), adsorption-free state (middle) and oxygen excess (right), demonstrating the change in relative volume of interfacial oxide and metal upon adsorption.

$$a_O^{(if\text{-}ox)} = a_{O2}^{(g)1/2}\exp\left(-\Delta G^{\circ adsox}/RT\right) = a_O^{(met)}\exp\left(-\Delta G^{\circ segox}/RT\right) \quad (5b)$$

At given oxygen activity, the chemical compositions of the coexisting bulk phases are known (aluminum and oxygen solubility in copper and transition metal solubility in alumina). In the coexistence range of copper and alumina phases, those solubilities are very small (10^{-4} for oxygen in copper,[9] $<0.1\%$ for aluminum in copper[10] and $<0.5\%$ for copper oxide in alumina[11] at 1100 °C and low oxygen activity). From those values and the activity coefficients in the binary systems follows that activities and mole fractions of copper in the metal phase and of alumina in the oxide solid solution are close to 1:

$$a_{Al_2O_3}^{(oxide)} \approx 1 \qquad \text{and} \quad a_{Cu}^{(metal)} \approx 1 \quad (6)$$

Concentrations of bulk point defects, such as vacancies and interstitials remain very small compared to 1.[12,13]

In the interfacial double-slab, the standard chemical potential in the interface slab $\mu_i^{\circ(if\text{-}met)}$ and $\mu_i^{\circ(if\text{-}ox)}$ are assumed to be the same as in the corresponding bulk metal and oxide, respectively. The number of total lattice sites in the interfacial double slab is constant, but the relative portion of interfacial metal and interfacial oxide phases varies with the relative oxygen excess/deficiency at the interface. Any adsorption of excess oxygen to the interface leads with the formation of interfacial oxide clusters to a growth of the oxide crystal and diminishes in size the interfacial metal crystal by the number of metal atoms used for the formation of those oxide clusters. Equally, any adsorption of excess aluminum produces shrinkage of the interfacial oxide crystal and growth of the interfacial metal slab. Shrinking interfacial slabs show no changes with respect to the corresponding bulk crystal, therefore, activities of their components are considered to be the same as in the corresponding bulk crystal. Growing interfacial slabs, in contrast, distinguish from their corresponding bulk crystal, because the interfacial clusters differ in composition from the usual bulk building elements. They are made of a mixture of regular bulk building elements and new interfacial building elements. In a first coarse approximation, ideal behavior of the interfacial defects can be assumed. However, for large oxygen excess (deficiency), the interfacial defect fractions are large, and a more sophisticated defect model is needed, which accounts for defect interactions.

3. Interface crystallography in alumina

In order to cope with the anisotropy of the solids in this continuum description, we have to consider the crystal structure of oxide, metal and interface, the relative orientation of the two crystals and the crystallographic position of the interfacial plane. For the model, we have to define then the interfacial slabs, their thickness and terminating planes.

In the above consideration not a crystallographically sharp (Gibbs) interface is considered, but a broader "chemical interface", in which segregation takes place. If only direct neighbor interactions are strong enough to produce Gibbs' adsorption to the interface, then alumina-metal interfaces have a typical width of 2–3 lattice planes. The interfacial metal slab is typically composed of one atomic layer and the interfacial oxide slab has a thickness representing the stoichiometric crystal.

The Young's modulus of metallic copper is much smaller than that of alumina.[14] At a semi-coherent interface, therefore, almost all lattice deformation will occur in the metal phase. As a result, the exact orientation of the metal and the lattice misfit do probably not play an important role for the adsorption processes at the interface as long as the copper plane is sufficiently dense-packed. For this reason, we will not precisely distinguish different copper terminations in the following.

For various dense planes of alumina, the composition of the oxide interfacial slab and possible terminations are derived from $R\bar{3}c$ crystal structure of alumina,[15] see Fig. 2 and Table 1.

The stacking perpendicular to the basal plane is composed of alternating cation- and anion-occupied planes, see Fig. 2a. Two different polar terminating planes can be distinguished, (0006-O) and (0006-Al), which are exclusively occupied by either cations or by anions. While the bulk plane densities are $10.2{\cdot}10^{18}$ Al atoms/m^2 and $15.6{\cdot}10^{18}$ O atoms/m^2, electroneutral surface and interface planes have only half that occupancy.

The stacking perpendicular to the prismatic planes $\{11\bar{2}0\}$ is made of alternating aluminum-occupied planes and ondulated oxygen-occupied planes, see Fig. 2b, providing then another family of polar interface planes.

According to the projection of the alumina structure along $[11\bar{2}0]$ in Fig. 2c, all prismatic planes $\{3\bar{3}00\}$ are neutral and identically occupied by a stoichiometric ratio of aluminum and oxygen ions, providing then a family of mixed neutral interfaces.

The 12 rhombohedral planes in alumina are divided in two families of planes (respecting the R$\bar{3}$c symmetry, but not the hexagonal symmetry!), the rhombohedral dense planes $\{\bar{1}102\}$ and the rhombohedral non-dense planes $\{3\bar{3}06\}$.

The projection along $[\bar{1}101]$ in Fig. 2d shows the alternating ABCB… stacking for the rhombohedral dense planes $\{\bar{1}102\}$, made of a plane of vacant octahedral sites, a mixed plane of aluminum and oxygen ions in ratio 1:1, a plane solely occupied by oxygen and again a mixed plane with Al/O = 1:1. This provides polar and mixed polar terminating planes. The rhombohedral

non-dense plane $\{3\bar{3}0\bar{6}\}$ stacking is composed of alternating cationic and anionic planes, Fig. 2e, and yields two different polar terminating planes.

Twelve structurally equivalent $\{11\bar{2}3\}$ planes occur in the alumina structure. For all of them, an alternating stacking of oxygen-occupied and mixed planes is observed, Fig. 2f, that provides polar and polar mixed terminating planes.

The number of possible interfaces between a crystalline metal and alumina is unlimited, however, only

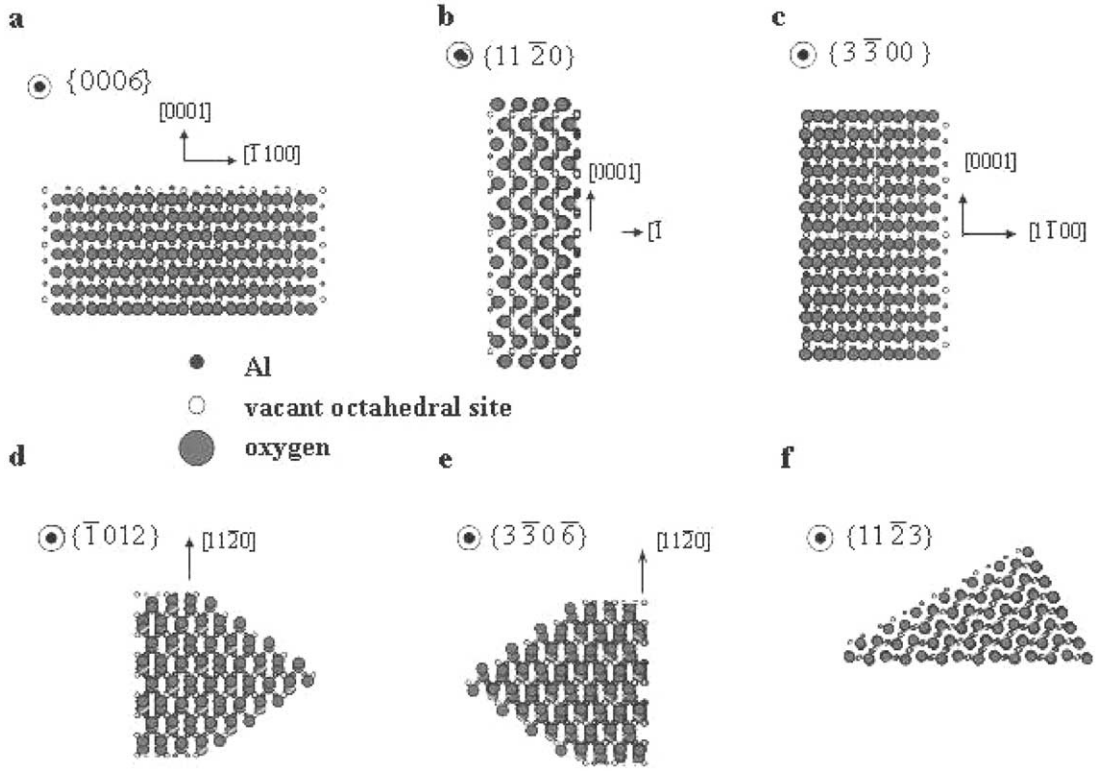

Fig. 2. Projections of the α-alumina structure showing the stacking perpendicular to the (a) basal plane {0006}, (b) prismatic plane $\{11\bar{2}0\}$, (c) prismatic plane $\{3\bar{3}00\}$, (d) dense rhombohedral plane $\{\bar{1}102\}$, (e) non-dense rhombohedral plane $\{3\bar{3}0\bar{6}\}$ and (f) pyramidal plane $\{11\bar{2}3\}$. Oxygen atoms are grey, aluminum atoms black, empty octahedral sites in the structure are indicated in light grey.

Table 1
Occupancies of different planes in bulk alumina (maximum occupancy) and at stoichiometric surfaces and interfaces

Families of interfacial planes (stacking)	Plane	Bulk plane occupancy	Stoichiometric surface or interface plane occupancy
{0001} alternating Al- and O-termination	(0001-Al)	10.2 10^{18}/m^2 Al^{3+}	5.1 10^{18}/m^{2}Al
	(0001-O)	15.6 10^{18}/m^2 O^{2-}	7.8 10^{18}/m^2 O^{2-}
$\{1\bar{1}00\}$	(1-100)	6.5 10^{18}/m^2 AI^{3+} +	
$\{11\bar{2}0\}$ alternating Al- and O-termination	$(11\bar{2}0$-Al)	11.2 10^{18}/m^2 Al^{3+}	5.6 10^{18}/m^2 Al^{3+}
	$(11\bar{2}0$-O)	16.8 10^{18}/m^2 O^{2-}	8.4 10^{18}/m^2 O^{2-}
$\{1\bar{1}02\}$	$(1\bar{1}02$-V)		–
(vacant plane), (mixed polar plane),	$(1\bar{1}02$-$mix_{pol})$	8.19 10^{18}/m^2 Al^{3+}	6.83 10^{18}/m^2 Al^{3+}
(polar anion plane), (mixed polar plane)		+ 8.19 10^{18}/m^2 O^{2-}	+8.19 10^{18}/m^2 O^{2-}
	$(1\bar{1}02$-O)	8.19 10^{18}/m^2 O^{2-}	4.095 10^{18}/m^2 O^{2-}
	$1\bar{1}02mix_{pol})$	8.19 10^{18}/m + Al^{3+}	6.83 10^{18}/m^2 Al^{3+}
		+ 8.19 10^{18}/m^2 O^{2-}	+8.19 10^{18}/m^2 O^{2-}
$\{1\bar{1}0\bar{2}\}$ $(1\bar{1}0\bar{2}$-Al), $(1\bar{1}0\bar{2}$-O)...	$(1\bar{1}0\bar{2}$-Al)	5.46 10^{18}/m^2 Al^{3+}	2.73 10^{18}/m^2 Al^{3+}
	$(1\bar{1}0\bar{2}$-O)	8.18 10^{18}/m^2 O^{2-}	4.095 10^{18}/m^2 O^{2-}
$\{11\bar{2}3\}$ $(11\bar{2}3$-Al), $(11\bar{2}3$-mix)...	$(11\bar{2}3$-Al)	4.9 10^{18}/m^2 Al^{3+}	2.45 10^{18}/m^2 O^{2-}
	$(11\bar{2}3$-mix)	4.9 10^{18}/m^2 Al^{3+}	4.9 10^{18}/m^2 Al^{3+}
		+14.7 10^{18}/m^2 O^{2-}	+ 7.35 10^{18}/m^2 O^{2-}

dense interfaces are worthwhile further considerations, since they have the lowest energies. Our systematic treatment shows, that we can classify the interfaces in three main groups, polar interfaces with a terminating plane being exclusively occupied by cations (or anions), mixed stoichiometric interfaces and polar mixed planes, which show mixed occupation, but do not respect the stoichiometric ratio. Mixed polar interface behavior can be understood as a combination of polar and mixed neutral plane behavior, so that finally the behavior of all interfaces can be deduced from that of polar and mixed stoichiometric planes, by scaling with the corresponding alumina plane densities.

4. Defect chemistry in the interfacial slab

For the bulk copper phase, the following structural elements are considered: neutral copper atoms, $Cu_{Cu}^{0(met)}$ and interstitial oxygen $O_i^{0\ (met)}$, presence of copper in an oxidation state close to 1^+, copper vacancies and substituional aluminum are neglected. The bulk oxide crystal has two sublattices, a cationic sublattice, occupied by $Al_{cat}^{(ox)}$, $V_{cat}^{(ox)}$ and substitutional $Cu_{cat}^{(ox)}$ in different charge states, and an anionic sublattice, occupied by oxygen ions $O_O^{2-\ (ox)}$ and oxygen vacancies $V_O^{0\ (ox)}$.

The interfacial slabs have the same structural units as the bulk phases and in addition the typical interfacial defects: structural vacancies and interfacial charge transfer clusters. "Structural vacancies" are typical interfacial defects that do not exist in the bulk crystals; they correspond to vacant sites on cation or anion crystal positions in the terminating oxide plane and form at the interface for reasons of electroneutrality. In strict terms, they cannot be part of a regular bulk oxide lattice. They can be considered as a lattice hole or strained region in the alumina crystal. They will be notated as V_{st} to distinguish from regular cation and anion vacancies. As building units of the bi-crystal, they can be associated with a formation energy; here, this energy is approximated by the volume-correspondent portion of the formation energy of an associated Schottky pair (missing lattice molecule) in alumina (E^{sch}).[16]

Two types of interfacial charge transfer clusters form by interaction between the two phases at the interface: oxide clusters $\{2Cu_{Cu}^{1+}—O_O^{2-}\}^{(if\text{-}ox)}$ and metal clusters $\{xCu_{Cu}—Al_{Al}\}^{(if\text{-}met)}$, see Fig. 3.

Defect concentrations in the interfacial slab may differ from the corresponding bulk concentrations. (Since the two bulk phases do not have a common sublattice and are very different, we use a notation with effective charges for the defects and species instead of the common Kroeger-Vink notation.)

Mass [Eqs. (8a–c) for metal and (10a–c) for oxide], site [Eq. (9)] and charge balances [Eq. (13)] are established for the slabs. Square brackets indicate the fractions of the total regular plane concentration.

$$x_{Cu}^{(if\text{-}met)} = \left[Cu_{Cu}^{0}\right]^{(if\text{-}met)} + 3[\{Cu_3Al\}]^{(if\text{-}met)} \tag{8a}$$

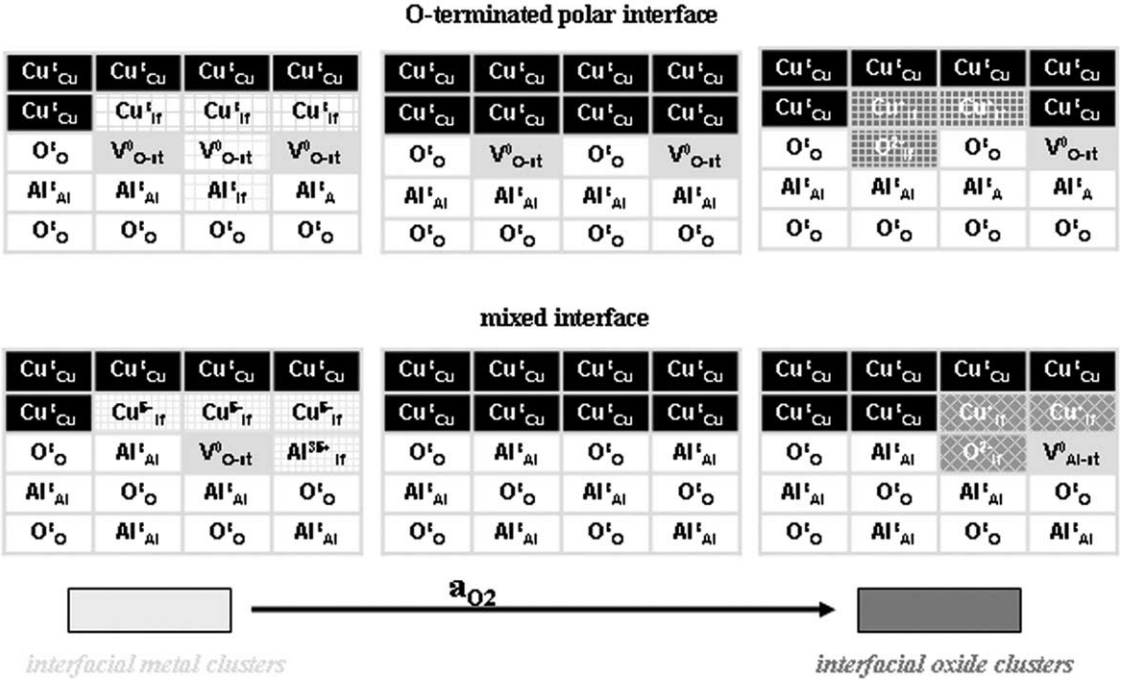

Fig. 3. Schematic presentation of the majority interfacial defects at the alumina–copper interface for (a) oxygen deficiency, (b) adsorption-free state, (c) oxygen excess. Interfacial oxide clusters are shaded in dark grey, interfacial metal clusters in light grey.

$$x_{Al}^{(if\text{-}met)} = \left[Al_{Cu}^{0}\right]^{(if\text{-}met)} + \left[\{Cu_3Al\}\right]^{(if\text{-}met)} \text{with} \left[Al_{Cu}^{0}\right]^{(met)} << \quad (8b)$$

$$x_{O}^{(if\text{-}met)} = \left[O_{iCu}^{0}\right]^{(if\text{-}met)} \quad (8c)$$

$$\left[Cu_{Cu}^{0}\right]^{(if\text{-}met)} + \left[Cu_{Cu}^{1+}\right]^{(if\text{-}met)} + \left[V_{Cu}^{0}\right]^{(if\text{-}met)} = 1 \quad \text{with} \left[V_{Cu}^{0}\right]^{(if\text{-}met)} << \quad (9)$$

$$x_{Al}^{(if\text{-}ox)} = \left[Al_{cat}^{3+}\right]^{(if\text{-}ox)} \quad (10a)$$

$$x_{O}^{(if\text{-}ox)} = \left[O_{O}^{2-}\right]^{(if\text{-}ox)} + \left[\{Cu_2O\}\right]^{(if\text{-}ox)} + \left[V_{O\text{-}st}^{0}\right]^{(if\text{-}ox)} \quad (10b)$$

$$x_{Cu}^{(if\text{-}ox)} = 2\left[\{Cu_2O\}\right]^{(if\text{-}ox)} \quad (10c)$$

$$\left[Al_{cat}^{0}\right]^{(if\text{-}ox)} + \left[Al_{cat}^{3+}\right]^{(if\text{-}ox)} + \left[V_{cat}^{0}\right]^{(if\text{-}ox)} + \left[V_{cat}^{0}\right]^{(if\text{-}ox)} = 1; \quad \left[V_{cat}^{0}\right]^{(if\text{-}ox)} \approx 0 \quad (11)$$

$$\left[O_{O}^{2-}\right]^{(if\text{-}ox)} + \left[V_{O\text{-}st}^{0}\right]^{(if\text{-}ox)} + \left[V_{O}^{0}\right]^{(if\text{-}ox)} = 1 \quad \text{with} \left[V_{O}^{0}\right]^{(if\text{-}ox)} << \quad (12)$$

$$2\left[Cu_{Cu}^{1+}\right]^{(met)} + \left(3\left[O_{O}^{2-}\right]^{(ox)} - 2\left[Al_{Al}^{3+}\right]^{(ox)}\right) = 0 \quad (13)$$

Equations for the formation of the interfacial clusters write as

$$2\ Cu_{Cu}^{0(if\text{-}met)} + O_{O}^{0} \Longleftrightarrow \left\{2\ Cu_{Cu}^{1+(if\text{-}met)\cdots} O_{O}^{2-(ox)}\right\} \quad (14)$$

$$3\ Cu_{Cu}^{0(if\text{-}met)} + Al_{cat}^{0(if\text{-}ox)} \Longleftrightarrow \left\{3\ Cu_{Cu}^{\delta-(if\text{-}met)\cdots} Al_{cat}^{3\delta+(if\text{-}ox)}\right\} \quad (15)$$

Excess oxygen can be introduced into the oxide interfacial slab by different ways. For polar interfaces with a partially filled terminating oxygen plane, the structural vacancies in this plane, $V_{O\text{-}st}^{0(if\text{-}ox)}$, can be occupied by oxygen, which diffuses from the gas phase through the bulk metal phase to the interface [Eq. (16)]. At mixed neutral interfaces, no such structural vacancies exist; relative oxygen excess can only be obtained by decomposition of interfacial alumina building units, see Eq. (17), when aluminum leaves the crystal via diffusion through the bulk phases and the remaining excess oxygen interacts with copper under formation of an interfacial oxide cluster.

$$6\ Cu_{Cu}^{0(if\text{-}met)} + 3V_{O\text{-}st}^{0(if\text{-}ox)} + 3/2O_2(gas) \Longleftrightarrow 3\left\{2Cu_{Cu}^{1+(if\text{-}met)\cdots} O_{O}^{2-(ox)}\right\} + 2V_{cat\text{-}st}^{0} + 3\ Al^{0(gas)} \quad (16)$$

$$6\ Cu_{Cu}^{0(if\text{-}met)} + Al_2O_3^{(if\text{-}ox)} \Longleftrightarrow 3\left\{2\ Cu_{Cu}^{1+(if\text{-}met)\cdots} O_{O}^{2-(ox)}\right\} + 2V_{cat\text{-}st}^{\circ} + 3\ Al^{0(gas)} \quad (17)$$

For oxygen deficiency, metallic aluminum-copper clusters $\{3\ Cu_{Cu}^{\delta\text{-}(if\text{-}met)\cdots} Al_{cat}^{3\delta+\ (if\text{-}ox)}\}$ are formed. At polar aluminum-terminated interfaces, such clusters form by adsorption of excess aluminum from the gas phase, $Al^{0(gas)}$, to structural vacancies $V_{cat\text{-}st}$, see Eq. (18). At mixed stoichiometric interfaces, no such vacancies are present, and metallic clusters form by decomposition of alumina lattice molecules $Al_2O_3^{(if\text{-}ox)}$ under out-diffusion of oxygen through the metal phase to the gas $O_2^{(gas)}$, Eq. (19)

$$3\ Cu_{Cu}^{0(if\text{-}met)} + Al^{(gas)} + V_{cat\text{-}st}^{0(if\text{-}ox)} \Longleftrightarrow \left\{3\ Cu_{Cu}^{\delta\text{-}(if\text{-}met)\cdots} Al_{cat}^{3\delta+(if\text{-}ox)}\right\} \quad (18)$$

$$6\ Cu_{Cu}^{0(if\text{-}met)} + Al_2O_3^{(if\text{-}ox)} \Longleftrightarrow 2\left\{3\ Cu_{Cu}^{\delta\text{-}(if\text{-}met)\cdots} Al_{cat}^{3\delta+(ox)}\right\} + 3V_{O\text{-}st}^{\circ} + 3/2O_2^{(gas)} \quad (19)$$

5. Gibbs' adsorption isotherms

The complete set of equations for the interfacial point defect model has been described in the precedent paragraph. For its solution, a solution model for the interfacial defects and their formation energies in Eqs. (14)–(19) are needed. For small deviations in the interfacial defect concentrations form those of the reference stoichiometric interface, ideal behavior can be assumed for the

interfacial defects and regular lattice species, and, instead of activities, concentrations of those species can be used and interrelated. For larger deviations from the stoichiometric reference state of the interfaces, non-ideal defect behavior has to be considered.

Different contributions to the adsorption energies can be identified: The main contribution is the energy of formation of the new bond across the interface. In lack of a better approximation, in this empiric approach, this energy is approximated (despite the existing differences in symmetry) by the macroscopic energy of formation of the corresponding bulk phases, bulk Cu_2O with $\Delta H^f(Cu_2O)$[17] for the oxide cluster and bulk $(Cu_{0.75}Al_{0.25})$ with $\Delta H^f(Cu_{0.75}Al_{0.25})$,[17] for the metallic cluster. Bulk phase thermodynamics indicate that $CuAlO_2$ forms as reaction product at Cu–alumina interfaces at low oxygen activity. Then, the interfacial oxide cluster could be composed of $CuAlO_2$ and not of Cu_2O. Since the energies of formation of Cu_2O and $CuAlO_2$ are very close, the precise atom arrangement at the interface will probably determine the exact type of interfacial cluster. For polar interfaces, the $CuAlO_2$ bulk symmetry does not provide a suitable geometry for the interface cluster, therefore, such mixed oxide interfacial clusters are not further considered. The interfacial clusters form on the crystal lattice of alumina, therefore, they are expected to adopt an ordered solid-like structure (as thin liquid films on solid surfaces).[18] For this reason, in our computation, we use even for temperatures above the melting point of copper and cuprite the formation energies of solid clusters.

The adsorption processes are accompanied by a change in entropy. The adsorption entropy can be deduced from the configurational changes in the affected sublattice. The resulting energy contributions $RT\,\Delta S^{ads}$ remain small.

Differences in volume of the various interfacial lattice units are at the origin of adsorption stresses and a elastic energy contribution $E^{ads\text{-}elast}$ to the adsorption energy. The elastic energy usually increases with the excess. If, in our simple image of lattice site conservation, the adsorption of one oxygen atom provokes a certain elastic strain in the interfacial layer, this strain will double upon adsorption of a second atom and thus, for large oxygen excess, achieve very high values. However, the elastic energy contribution, we have to account for, can be smaller than that obtained from the volume differences between the various interfacial lattice units, if stresses relax. For interfaces with liquid metals, viscous relaxation occurs at the interface and adsorption stresses remain negligible. A similar situation is encountered for glass-metal interfaces because of the viscous flow of the glass. At interfaces between two solid crystals with rigid lattices, little relaxation is possible, and adsorption stresses reach a maximum value, corresponding to the theoretical volume change at the interface. Most interfaces will be situated between the extreme cases of complete and no stress relaxation. Therefore, in this work, we will compute the two extreme cases and thus demonstrate the whole range in behavior. A maximum strain energy contribution is estimated from the energy necessary to form/annihilate the equivalent volume of Schottky associated vacancy pairs in bulk alumina $\{2V^x_{cat}\ 3V^x_O\}$ indicated in;[16] this value definitely overestimates the elastic energy at the interface.

In defect models, any concentration-dependency of the defect formation energies is usually expressed in form of activity coefficients of the defects. In order to reach the common description, we can transform our set of defect equilibria, use activity coefficients and concentration-independent formation energy. Then it is even more obvious that the activity coefficients induce only for large oxygen excess a deviation form the ideal behavior and that this difference increases with the deviation from stoichiometry.

Table 2 summarizes adsorption energies used in the computation for 1400 K. Figs. 4 and 5 present the adsorption isotherms for crystallographically different interfaces at two temperatures, which represent solid and liquid copper. All isotherms show an adsorption-free plateau and adsorption branches with relative oxygen excess at high oxygen activity and with relative oxygen deficiency at low oxygen activity. Oxygen deficiency at the interface is only obtained close to the lower stability limit of the interface ($a_{O2} < 10^{-26}$ at 1400 K) and the absolute values remain small. Oxygen excess forms more readily for all interfaces at $a_{O2} > 10^{-12}$ at 1400 K and $a_{O2} > 10^{-16}$ for 1200 K. For all interfaces, saturation is reached within the stability range. A comparison of the different interfaces shows that adsorption occurs earlier for polar interfaces. This effect is enhanced if stresses build up upon adsorption. In Figs. 4 and 5, adsorption isotherms are compared for stress-free and strained adsorption: solid curves were obtained by using for the adsorption energies solely bulk enthalpies, dotted curves when considering in addition the adsorption entropy and dashed curve, when adding in addition the strain energy contribution. While the adsorption branches on the low oxygen activity side change little for the different assumptions, significant differences are noticed for high oxygen activities. The entropy contribution yields only a small change in the adsorption branches. The adsorption stresses, however, produce a widening of the adsorption range over a much larger oxygen activity range, with an onset of adsorption being shifted by up to three orders of magnitude of a_{O2}.

Comparison of Cu-alumina interfaces with different terminating alumina planes shows that basal, prismatic and rhombohedral planes all achieve high relative oxygen excess concentrations in the high oxygen activity

range. The highest oxygen excess concentrations are achieved by adsorption of oxygen for prismatic $\{11\bar{2}0\}$ planes, followed by the basal plane {0006}. Highest aluminum deficiency is obtained by desorption of aluminum for the $\{11\bar{2}3\}$ planes, followed by the mixed polar rhombohedral $\{\bar{1}102\}$ planes and the prismatic $\{3\bar{3}00\}$ planes, see Fig. 6. The low density rhombohedral planes $\{\bar{1}10\bar{2}\}$ and other non-presented low density planes show much lower relative oxygen excess. It is once more visible that oxygen adsorption starts at lower oxygen activities than the aluminum desorption. The comparison of Fig. 6a computed for stress-free adsorption and Fig. 6b computed for conditions with uncompensated adsorption stresses shows that the difference in onset for oxygen adsorption and onset of aluminum desorption is diminished in presence of adsorption stresses. The curves for the different interfaces the show more and more overlapping. For liquid copper/alumina interfaces, however, the results obtained for stress-free adsorption are probably the most suitable approach, since the liquid metal allows rapid relaxation of all stresses at the interface. Atom densities (oxygen and aluminum) in the terminating alumina plane are presented in Fig. 7 (for negligible adsorption stresses). Fig. 7 demonstrates, that even though an important relative oxygen excess is established by aluminum desorption at the rhombohedral mixed polar $\{\bar{1}102\}$ plane, the resulting atom density at the highest oxygen activities in the thermodynamic stability range is low and does not favor the formation of this interface. Polar

Table 2
In put data used for the computation of Gibbs adsorption isotherms at 1400 K

Input data used for the computation of Gibbs adsorption at alumina–copper interfaces
$T = 1400$ K
Thermodynamic stability range $10^{-30.5} < a_{O2} < 10^{-6}$
$R = 8.3\ 14$ J/mol K
Formation enthalpy of metastable Cu_3Al (extrapolated): −15,500 J/mol
Gibbs free energy of formation of bulk alumina: −1229,322 J/mol
Formation enthalpy of metastable solid Cu_2O: −149,700 J/mol
Gibbs free energy of formation of vacant lattice molecules (associated Schottky pair) in bulk alumina: $E^{\text{Schottky}} = 150{,}000$ J/mol
Adsorption entropy = difference in entropy of the mixture between regular laatice units and interfacial defects after and before adsorption
Contribution of the adsorption stresses to the adsorption energy: $\Delta E_{\text{Stress}} = \Delta V / V^{\text{mol}}_{Al_2O_3} \times E^{\text{Schottky}}$

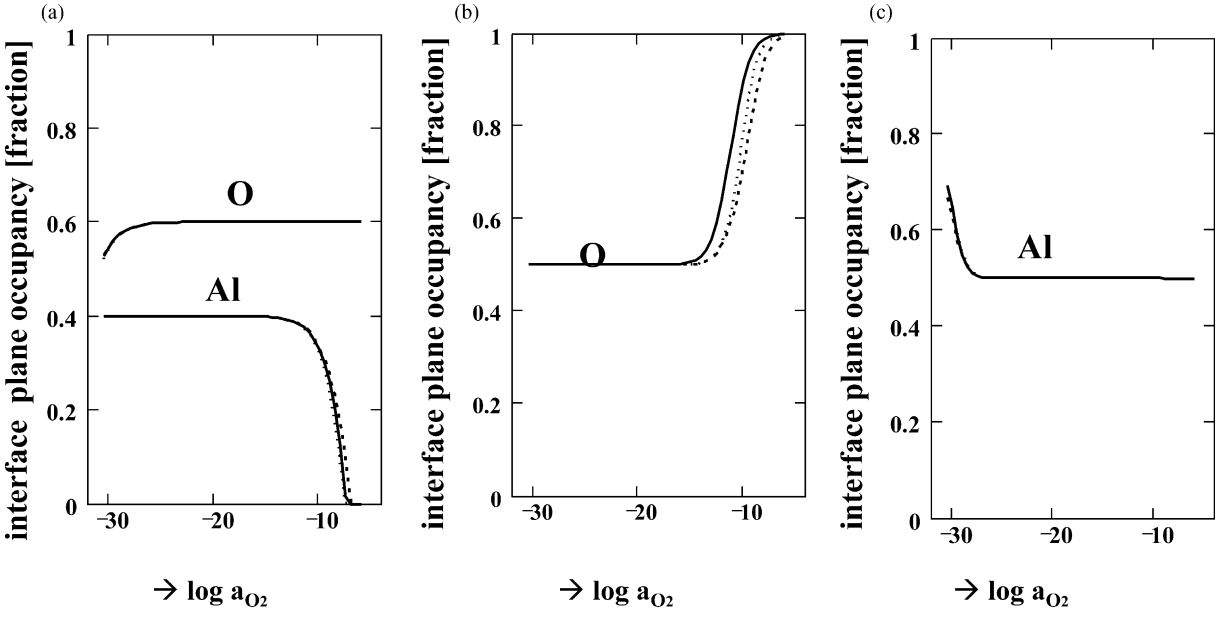

Fig. 4. Liquid Cu–α-alumina interface at 1400 K; predicted relative occupancies of the terminating alumina plane as function of oxygen activity. The behavior of different types of interfaces is presented: interfaces with mixed stoichiometric terminating oxide plane (a), polar oxygen terminating oxide plane (b) and polar aluminum terminating oxide plane (c). Solid, dotted and dashed curves are obtained with different assumptions for the adsorption energies: the solid curves are obtained when the adsorption energy is solely approximated by the formation enthalpy of corresponding bulk phases, the dotted one, when in addition an adsorption entropy is considered and dashed one, when in addition adsorption stresses due to changes in volume upon adsorption are taken into account.

prismatic $\{11\bar{2}0\}$ and basal $\{0006\}$ planes develop a higher atom density upon adsorption and, therefore, are expected to form low energy Cu–alumina interfaces at high oxygen activity. In the plateau range, mixed terminating interfaces, such as found in the $\{\bar{1}102\}$, $\{3\bar{3}00\}$ and $\{11\bar{2}3\}$ families possess much higher atom densities and are expected to constitute the low energy interfaces. Effects of the resulting atom densities on the adsorption behavior are better reflected when modeling uncompensated adsorption stresses.

Integration of the excess concentration curves yields the decrease in free energy of the interfaces by adsorption. Results are presented in Fig. 8. Notice that a substantial decrease in energy is obtained for all dense planes, which ranges between 0.5 and 1.4 J/m^2. It can be seen that the decrease in specific interfacial free energy due to Gibbs adsorption includes as key determining factor the onset of adsorption for the type of activated adsorption mechanism and the plane density. At the upper limit of the stability range, the energy decrease

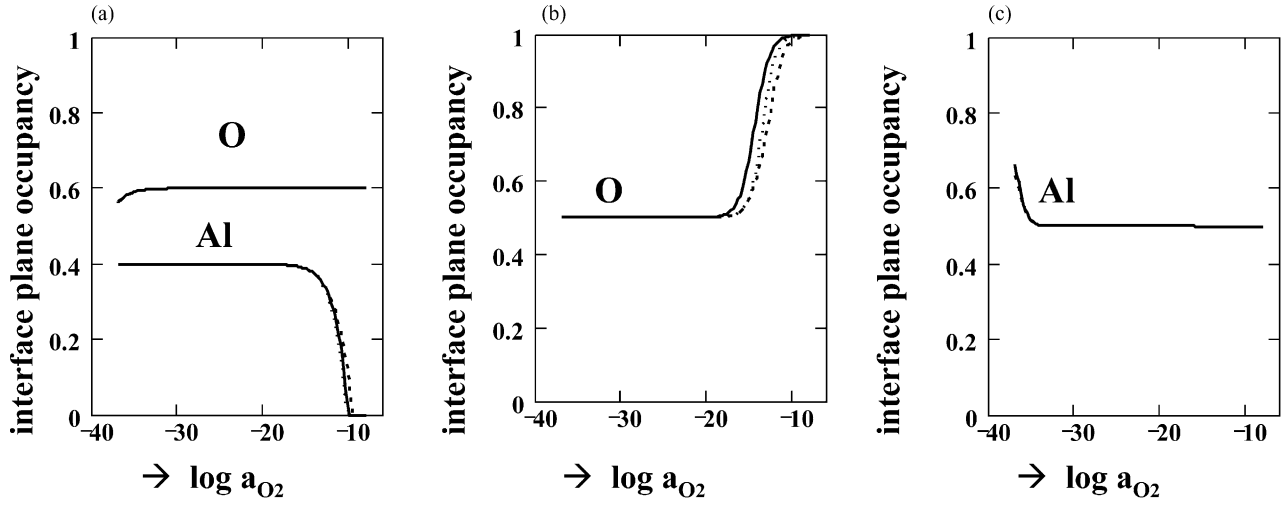

Fig. 5. Solid Cu–α-alumina interface at 1200 K; predicted relative occupancies of the terminating alumina plane as function of oxygen activity. The behavior of different types of interfaces is presented: interfaces with mixed stoichiometric terminating oxide plane (a), polar oxygen terminating oxide plane (b) and polar aluminum terminating oxide plane (c). Solid, dotted and dashed curves are obtained with different assumptions for the adsorption energies: The solid curves are obtained when the adsorption energy is solely approximated by the formation enthalpy of corresponding bulk phases, the dotted one, when in addition an adsorption entropy is considered and dashed one, when in addition adsorption stresses due to changes in volume upon adsorption are taken into account.

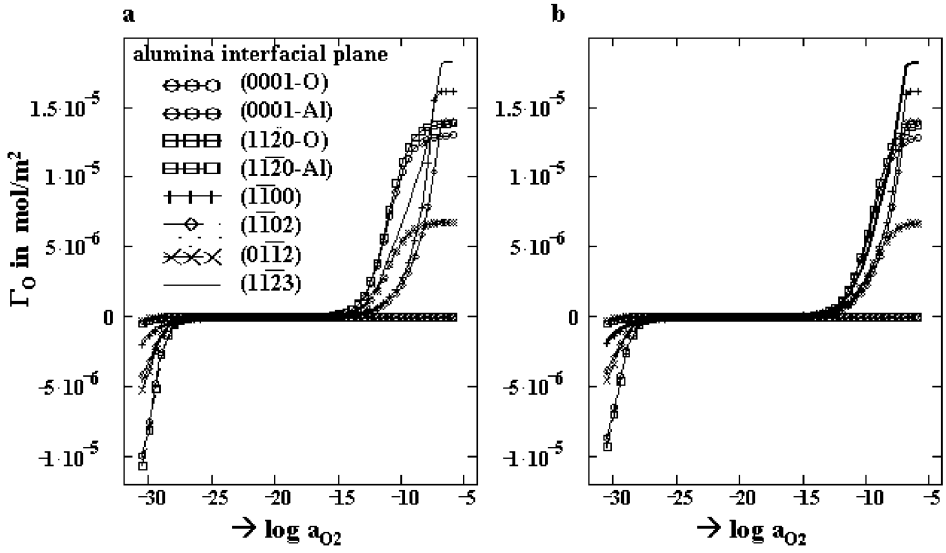

Fig. 6. Cu–α-alumina interface at 1400 K; model predictions on oxygen and aluminum excess concentrations in the terminating oxide plane as function of oxygen activity for various dense alumina–copper interfaces. (a) Model predictions for the limiting case of negligible adsorption stresses, (b) model predictions for the limiting case, where changes in volume upon adsorption are fully uncompensated and lead to adsorption stresses.

achieves about 1.5 J/m^2 for the pyramidal planes $\{11\bar{2}3\}$, −1 J/m^2 for the basal {0001}, prismatic $\{11\bar{2}0\}$ and dense rhombohedral planes $\{\bar{1}102\}$. The decrease in energy for the mixed prismatic planes $\{1\bar{1}00\}$ and the low density rhombohedral planes $\{\bar{1}10\bar{2}\}$ remains by 0.2 J/m^2 smaller. Fig. 8a is obtained for stress-free adsorption, while Fig. 8b reflects the effect of adsorption stresses. Again it can be seen that adsorption stresses diminish the global decrease in energy and the differences between the different interfaces.

Fig. 8a and b also show that the decrease in specific free interfacial energy in the low oxygen activity range remains negligible for all interfaces.

Excess oxygen or aluminum in the terminating oxide plane impose a negative or positive surface charge on the alumina crystal and induce the formation of a space charge layer in the oxide, in which the distribution of ionic and electronic defects compared to the bulk is altered. The exact concentrations of defects are derived from the condition of constant electrochemical potential across the entire oxide crystal, including the space charge layer. The general approach is described in Ref. 18. It has been applied by the author to MgO–Cu interfaces,[6] showing that the typical width of the space charge layer for high excess concentrations is only in the order of a few atomic planes, while it extends for very

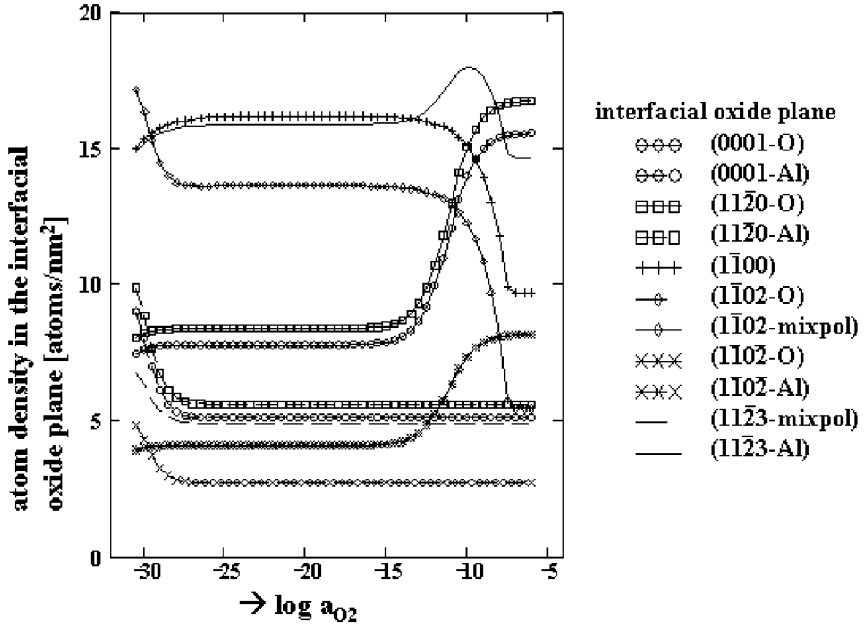

Fig. 7. Cu–α-alumina interface at 1400 K; model predictions on the atom (sum of oxygen and aluminum atoms) density in the terminating oxide plane as function of oxygen activity for various dense alumina–copper interfaces. (a) Model predictions for the limiting case of negligible adsorption stresses, (b) model predictions for the limiting case, where changes in volume upon adsorption are fully uncompensated and lead to adsorption stresses.

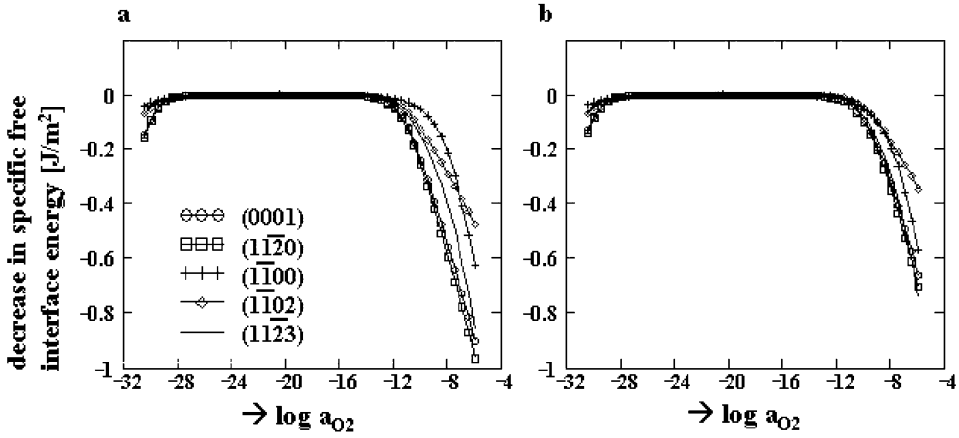

Fig. 8. Cu–α-alumina interface at 1400 K; model predictions on the relative decrease in interface specific free energy as function of oxygen activity for various dense alumina–copper interfaces; (a) Model predictions for the limiting case of negligible adsorption stresses, (b) model predictions for the limiting case, where changes in volume upon adsorption are fully uncompensated and lead to adsorption stresses.

small excess concentrations up to 10 nm. In the metallic half-crystal, continuity of the electrochemical potential is also respected and the charge spreads into the metal. The defect concentration profiles are not calculated in the present work, but are close to those in Ref. 6.

6. Comparison of model predictions to experimental results from the literature

In this last Section, model predictions are compared to different experimental results on Cu–alumina interfaces, local ELNES measurements at the interface allowing to detect the interfacial bond character.[19–22] wetting angle measurements[23–26] and precipitate equilibrium Wulff shapes.[27]

6.1. Comparison to ELNES results

ELNES studies have been realized for differently prepared interfaces[19–22] and allowed to elucidate interfacial electronic structure and bond character. The interfacial electronic structure can be compared to model predictions on the interfacial excess concentrations, since any interfacial excess goes hand in hand with a redox-reaction. Formation of Cu_2O interfacial clusters should show in the interfacial ELNES an increased white line intensity in the Cu L edge and O pre-peak, which both reflect the hybridization of Cu 3d and O 2p states. Metallic interfacial clusters are expected to also produce their typical features in the interfacial EELS spectrum, however, the oxygen activity range, where these clusters are expected to form, is experimentally difficult to be accessed. Numerous of the investigated Cu-alumina interfaces have been prepared by MBE[19–21] and therefore do not reflect the equilibrium chemistry. However, it is interesting to notice that different post-treatments of the interface resulted in modifications in the interfacial electronic structure.[19,21] As-processed interfaces show no significant hybridization of Cu 3d and O 2p states,[19] but after special post-treatment with ion-bombardment and high temperature annealing, differences were observed.[21] Some still unpublished results were obtained for Cu–alumina interfaces produced by internal oxidation of (Cu,Al) alloys at 900 °C and different oxygen activities.[22] Even though mainly γ-alumina forms during internal oxidation, for restricted conditions, also α-alumina precipitates were obtained with either dominating basal or prismatic facets. ELNES of those interfaces revealed a very important hybridization of Cu 3d and O 2p states with characteristic Cu_2O-like edge features at oxygen activity 10^{-8}, while at $a_{O2}=10^{-14}$ only a weak oxygen pre-peak was observed and an associated Cu L edge modification, which did not show the sharp white line of Cu_2O, but a broadened peak located at slightly higher (+1.8 eV) energy. Measurements at other oxygen activities are still in course.

6.2. Comparison to wetting of alumina by liquid Cu

Wetting angles for liquid copper on alumina are reported in Refs. 23–26; they range from 130 to 110° and show a strong dependency on the oxygen chemical potential. In Fig. 9, an attempt was made to superpose our model predictions on adsorption-related decrease in interfacial energy and the experimental results on (γ^{sl}–γ^{sv}) of Ref. 23 (replotted from Ref. 23 and fitted by vertical shift, since γ^{sv} = constant). It is not surprising that model predictions obtained for stress-free adsorption fit best the experimental results, because liquid copper is expected to allow a rapid accommodation of adsorption-related changes in volume. Perfect agreement between experiments and model is found for the onset of adsorption. In Ref. 23, a discontinuity in the experimental (γ^{sl}–γ^{sv}) results is evoked, which could be interpreted in terms of an interfacial phase transformation. The present model does not consider any interfacial phase transformations and cannot give any hint on that subject. However, the predicted decrease in energy at high oxygen activity is in the same order of magnitude as the experimentally measured one. Scattering in the experimental wetting angles is important in the oxygen activity range, for which the interface phase transformation was suggested; therefore, it is difficult to judge if such transformation has to be assumed or whether the experimental results can solely be interpreted by the present model. The experimental points seem to fit the computed curve for simple adsorption. It shall be recalled, that the experimental alumina surface in the wetting experiments was close to the basal plane of alumina, but did not have the perfect orientation. Therefore, the experimentally measured decrease in interfacial

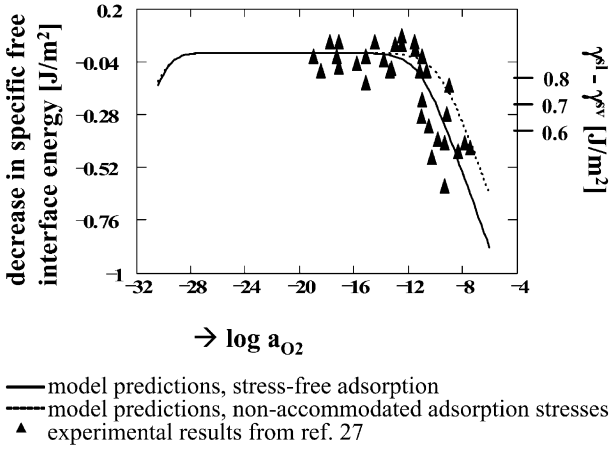

Fig. 9. Comparison of model predictions on the adsorption-related decrease of interfacial energy at liquid Cu–alumina interfaces at 1400 K (basal plane) to experimental wetting results (γ^{sl}-γ^{sv}) from Ref. 23.

energy is expected to be slightly smaller than the values predicted for an atomically flat interface.

6.3. Comparison to equilibrium precipitate shapes

The predictions of the adsorption model can also be compared to the evolution with oxygen activity in equilibrium shape of oxide precipitates in metals or metal precipitates in oxides.[8] Unfortunately, internal oxidation of (Cu,Al) alloys produces mainly small γ-alumina particles and only in a very restricted temperature and oxygen activity domain large-size α-alumina.[27] Alumina cannot be doped with sufficient copper oxide, to allow for precipitation of copper by internal reduction. Implantation of copper into alumina produces small precipitates,[28] but no systematic study on precipitate shape as function of oxygen activity has been done. Preliminary studies in Ref. 27 suggest, that precipitates are solely limited by basal and prismatic $\{11\bar{2}0\}$ planes at high oxygen activity, while, in the plateau range, various different facets of similar sizes are present, similar to those describing the equilibrium pore shape in alumina.[29]

7. Conclusions

Gibbs adsorption of oxygen at α alumina- transition metal interfaces is modeled by continuum thermodynamics. Constraints due to adsorption-related changes in volume have been successfully handled in the model. It is stated that characteristic interfacial point defect clusters form at the interface and that their majority type and concentrations strongly depend on oxygen activity. Adsorption isotherms are modeled for typical data sets of liquid and solid copper. They show that, in an intermediate oxygen activity range, interfaces are made of stoichiometric alumina and metallic copper, while with increasing oxygen activity more and more excess oxygen is build into the interface and stabilized by a strong charge transfer interaction with copper. At the lower stability limit of the interface, oxygen deficiency establishes at the interface through formation of metallic clusters between aluminum and copper. According to the model, interfaces with different alumina planes exhibit different behavior, depending on the ''polarity'' and density of their interfacial oxide plane. While the various interfaces are expected to have very close energies in an intermediate oxygen activity range, at high oxygen activity, the energies of pyramidal, basal and prismatic $\{11\bar{2}0\}$ and dense rhombohedral alumina planes in contact with liquid (or solid) copper are considerably lowered by adsorption. Model prediction on the interfacial oxygen excess and the resulting decrease in interfacial free energy have been compared to ELNES results on Cu-alumina interfaces, to wetting behavior of alumina by liquid copper and to the precipitate shape evolution with oxygen activity in the metal-alumina systems. Good agreement between model and experimental results is achieved.

Acknowledgements

Financial support for this work was provided by Cornell University and Corning Incorporated. The author wants to thank A. Ferrand, CECM-CNRS, for preparing the images of the projected alumina structure.

References

1. Gibbs, J. W., *Scientific Papers I*. Dover Publ., New York, 1961.
2. Gibbs, J. W., *Scientific Papers I*. Dover Publ., New York, 1961.
3. Schmalzried, H., Navrotsky, A., *Chemical Kinetics of Solids*. Festkoeperthermodynamik, 1987, Verlag Chemie, Weinstein.
4. Saiz, E., Tomsia, A. P. and Cannon, R. M., Wetting and work of adhesion in oxide/metal systems. In *Ceramic Microstructures: Control at the Atomic Level*, ed. A. P. Tomsia and A. Glaeser. Plenum Press, New York, 1998, pp. 65–81.
5. Batyrev, I. G., Alavi, A. and Finnis, M. W., Equilibrium and adhesion of Nb/sapphire. *Phys. Rev. B*, 2000, **62**, 4698–4706.
6. Backhaus-Ricoult, M., Modeling of the Gibbs' adsorption at transition metal—oxide interfaces. *Phil. Mag*., 2001, **81**, 1759–1787.
7. Backhaus-Ricoult, M., Festkoerperreaktionen—Transport, Mechanismen und die Rolle von Phasengrenzen. *Nova Acta Leopoldina*, 2000, **NF83**(317), 127–154.
8. Backhaus-Ricoult, M., Wetting anisotropy and oxygen activity dependency for oxides by liquid transition metals studied through shape changes.... *Acta Mater*., 2001, **49**, 1747–1758.
9. Schmid, R., A thermodynamic analysis of the the Cu-O system with an associated solution model. *Metall. Trans*., 1983, **14B**, 473–481.
10. Massalski, T. B. and Okamoto, H., *Binary Alloy Phase Diagrams*. Metals Park, ASM int, 1990.
11. *Phase Diagrams for Ceramists* (compiled at the National Bureau of Standards), Columbus, Ohio, American Ceramic Society, 1964–1990.
12. Jacobs, P. W. and Kotomin, E. A., Defect energies for pure corundum doped with transition metal ions. *Phil. Mag. A*, 1993, 695–709.
13. Chaudron, G., *Monographie sur les Metaux de Haute Purete*. Masson et Cie, 1972.
14. Kingery, W. D., *Introduction to Ceramics*. Wiley, New York, 1982.
15. Lee, W. E. and Lagerloeff, K. P., Structural and electronic diffraction data for sapphire. *J. Electron microscopy Techn*., 1985, **2**, 247–258.
16. Jacob, K. T. and Alcock, C. B., Thermodynamics of CuAlO2 and CuAl2O4 and phase equilibria in the system Cu2O-CuO-Al2O3. *J. Am. Cer. Soc*., 1975, **58**, 192–195.
17. Barin, I. and Knacke, O., *Thermochemical Properties of Inorganic Substances*. Springer Verlag, Berlin, 1973.
18. Maier, J., Ionic conduction in space charge regions. *Progress in Sol. St. Chem*., 1995, **23**, 171–263.
19. Scheu, C., Dehm, G. and Ruehle, M. *et al*., Electron energy loss spectroscopy of Cu- alpha alumina interfaces grown by molecular beam epitaxy. *Philosophical Magazine*, 1998, **A78**, 439–465.

20. Scheu, C., Stein, W. and Ruehle, M., Electron energy loss near edge structure studies of a Cu/(11-20) alpha alumina interface. *Phys. Stat. Sol.*, 2000, **222**, 199–211.
21. Scheu, C., Dehm, G. et al., A combined approach of analytical and high resolution TEM to determine the interface structure of Cu/(11-20) alpha alumina. In *Proc. EUREM, 12th Congress on Electron Microscopy,* 2000, ed. Czech. Soc. Electron Microscopy, Prague.
22. Backhaus-Ricoult, M. and Trichet, M.-F., ELNES at different copper-alpha alumina interfaces. *Zeitschrift f. Metallkunde*, **94**, 250–258.
23. Ghetta, V., Fouletier, J. and Chatain, D., Oxygen adsorption isotherms at the surfaces of liquid Cu and Au-Cu alloys and their interfaces with Al2O3 detected by wetting experiments. *Acta Mater.*, 1996, 1927–1936.
24. Diemer, M., Neubrand, A., Trumble, K. and Roedel, J., Influence of the oxygen content on the wettability in the copper-oxygen-alumina system. *J. Am. Ceram. Soc.*, 1999, **82**, 2825–2832.
25. Ownby, P. D. and Liu, J. J., Surface energy of liquid copper and single crystal sapphire and the wetting behavior of copper on sapphire. *Adhes. Sci. Technol.*, 1988, **2**, 255.
26. Mehrotra, S. P. and Chaklader, A. C., Interfacial phenomena between molten metals and sapphire substrate. *Metall. Trans.*, 1985, **B16**, 567.
27. Backhaus-Ricoult, M., Trichet, M.-F., Morphology of internally oxidized (Cu,Al) (in preparation).
28. Farlow, G. C., White, C. W. and McHargue, C. J. *et al.*, The structure and properties of ion-implanted alumina. *Nucl. Instrumen. Methods Phys. Res.*, 1985, **B7/8**, 473.
29. Choi, J.-H., Kim, D.-Y., Hockey, B. J., Wiederhorn, S. M., Handwerker, C. A., Blendell, J. E., Carter, W. C. and Roosen, A. R., Equilibrium shape of internal cavities in sapphire. *J. Am. Ceram. Soc.*, 1997, 62–68.